Applied Catalysis B: Environmental 183 (2016) 149–158

Contents lists available at ScienceDirect

Applied Catalysis B: Environmental

journal homepage: www.elsevier.com/locate/apcatb

Glass fiber-supported TiO_2 photocatalyst: Efficient mineralization and removal of toxicity/estrogenicity of bisphenol A and its analogs

Boštjan Erjavec[a,*], Petra Hudoklin[b], Katja Perc[b], Tatjana Tišler[a], Marija Sollner Dolenc[b], Albin Pintar[a]

[a] Laboratory for Environmental Sciences and Engineering, National Institute of Chemistry, Hajdrihova 19, SI-1001 Ljubljana, Slovenia
[b] Chair of Pharmaceutical Chemistry, Faculty of Pharmacy, University of Ljubljana, Aškerčeva 7, SI-1000 Ljubljana, Slovenia

ARTICLE INFO

Article history:
Received 19 June 2015
Received in revised form
25 September 2015
Accepted 14 October 2015
Available online 19 October 2015

Keywords:
Immobilized TiO_2
Bisphenol analogs
Photocatalysis
Toxicity
Estrogenicity

ABSTRACT

Bisphenol A (BPA) and its analogs (BPF and BPAF) are a class of industrial chemicals that are proven to elicit endocrine disrupting effects, thus it is important to reduce their concentrations in effluent streams as much as possible. In this study, a simple and highly active glass fiber-supported TiO_2 photocatalyst was synthesized and applied in a UV-irradiated three-phase batch and continuous stirred-tank reactor (CSTR) for removal of toxicity and estrogenicity of water dissolved bisphenols. Bioassays of photocatalytically treated aqueous samples showed no estrogenic activity and complete removal of toxicity after 4 h of illumination, which was in accordance with high mineralization extent of bisphenols and their reaction derivatives. The photocatalytic examination of bisphenolic compounds revealed considerably higher stability of BPAF under UV light irradiation, due to two CF_3 groups attached to the central C atom. Moreover, these fluorinated groups were responsible for markedly higher toxicity of BPAF to crustaceans *Daphnia magna* in comparison to non-halogenated BPA and BPF, which manifested daphnids as excellent aquatic species for sensing fluorinated (halogenated) bisphenolic compounds. In addition, photocatalytic oxidation of bisphenol analogs in CSTR demonstrated feasibility of using the immobilized TiO_2 photocatalyst in continuous-flow light-assisted water purification systems. Detailed characterization of fresh and used photocatalysts confirmed substantial changes in active material structure. However, the corresponding impact on photocatalyst stability was found insignificant.

1. Introduction

Bisphenol A (BPA, 2,2-bis(4-hydroxyphenyl) propane), bisphenol F (BPF, bis(4-hydroxyphenyl) methane) and bisphenol AF (BPAF, 2,2-bis(4-hydroxyphenyl) hexafluoropropane) are a class of chemicals in which two phenolic rings are joined together through a bridging group that characterizes each particular compound. In BPA the bridging group is isopropylidene, while BPF differs from BPA only in virtue of its lack of two methyl groups on the central carbon atom. BPAF is a fluorinated analog of BPA, with two trifluoromethyl groups attached to the central carbon atom (Fig. 1) [1].

Bisphenols (BPs) have been extensively used in industry as intermediates in the production of polycarbonate, epoxy, and corrosion-resistant unsaturated polystyrene resins. The resins are fundamental components of high quality commercial polymer materials used in a wide range of essential applications from electronics to food protection [2]. As a result, large amount of bisphenols has been released into the environment and numerous studies have confirmed their presence in surface waters, municipal wastewaters, wastewater treatment plant (WWTP) effluents and sewage sludge [3–5].

Although bisphenols have been in use for more than a century, account has only recently been taken of human exposure or potential consequential health risks. BPA is regarded as an endocrine disrupting compound (EDC) that causes adverse effects on reproduction and development, neural networks, and cardiovascular, metabolic, and immune systems in humans [5]. BPA exhibits estrogenic activity even at concentrations below 1 ng/L, thus it is important to reduce its concentration in the environment as much as possible [6]. Comparable acute toxicity, genotoxicity and estrogenic activity were reported for BPF [7–10], while exposure to BPAF exhibits higher biological activities [8,11], including stronger estrogenic activity according to in vitro MVLN assay and in vivo vitellogenin assay [12], activation of the human pregnane X receptor, a nuclear receptor that functions as a regulator of xenobiotic

* Corresponding author. Fax: +386 1 47 60 460.
E-mail address: bostjan.erjavec@ki.si (B. Erjavec).

http://dx.doi.org/10.1016/j.apcatb.2015.10.033
0926-3373/

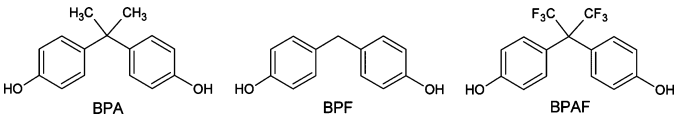

Fig. 1. Chemical structures of bisphenols used in this study as model pollutants.

[13] and testosterone reduction by directly affecting testis function in adult male rats [14].

Nowadays, the major sources of pollution with bisphenols are continuous emissions of wastewaters, e.g., landfill leachates and industrial effluents, which are usually sent to wastewater treatment plants and treated to the unsatisfactory extent [15]. As a consequence, various methods have been developed for more efficient removal of bisphenols from wastewaters, such as physical removal, biodegradation, and advanced oxidation processes (AOPs). Among these, AOPs are regarded as one of the most effective treatment technologies, due to in-situ generation of highly reactive radical species for degrading water contaminants. Among bisphenol analogs that are in commerce, BPA has been by far the most widely studied in versatile AOP systems, including photocatalytic oxidation, catalytic wet air oxidation (CWAO), ozonation, photo-Fenton oxidation, ultrasonic cavitation, UV/H_2O_2, etc., and fair to high efficiencies were reported [16–20]. On the other hand, only few attempts to eliminate either BPF or BPAF from aqueous solutions were reported so far. Liu et al. [21] examined UV-A light assisted photodegradation of BPAF and reported 78% conversions of TOC in the presence of acid-activated montmorillonite KSF. Moreover, MWCNTs as sorbent were used for separation of trace amount of BPAF from wastewater samples and 95% recoveries in ethanol were reported [22]. Lu et al. [23] suggested MnO_2-mediated oxidation as an effective treatment method for potential removal of BPF from wastes before their release into the environment. In addition, BPF was also effectively oxidized by horseradish peroxidase (HRP), especially, if the reaction was catalyzed in the presence of H_2O_2 and poly(ethylene glycol) [24].

Heterogeneous photocatalysis is a representative of AOPs and has proved to be of real interest as an efficient tool for degrading aquatic [25–27], atmospheric [28–30] and microbial [31] contaminants. The initial step in heterogeneous photocatalysis is generation of electron–hole pairs by light activation of semiconductor material. The photogenerated electron–hole pairs are requisite for the formation of reactive species, i.e., hydroxyl radicals (•OH), which facilitate the degradation of organic components. Ideally, during this process organic pollutants are mineralized to carbon dioxide, water and mineral acids [32]. Titania (TiO_2) is the most widely studied semiconductor photocatalyst in numerous environmental applications, due to its excellent photoactivity, physical and chemical stability, low cost and easy access. Usually, it is found in a powdered form and applied as a slurry catalyst, i.e., titanium dioxide powder suspended in polluted water. However, the post-treatment separation of TiO_2 powder from the treated water inevitably increases the cost of water purification process; therefore, immobilized photocatalysts appear to be more prosperous in light-assisted water treatment technologies, especially those that run around the clock [33]. In addition, the quantum yields of the two systems are comparable, which makes the immobilized systems even more attractive [34]. The overall performance of the latter is affected by various factors, such as synthesis conditions, immobilization procedures, and support type and shape [35].

In the present study, immobilized TiO_2 photocatalyst was synthesized by a routine preparation procedure, thoroughly characterized and subsequently applied in a UV irradiated three-phase batch and continuous stirred-tank reactor (CSTR) for removal of toxicity and estrogenicity of water dissolved BPs (bisphenol A, F and AF). Titania photocatalyst was supported by non-woven glass fibers (GF), which are flexible, offer high specific surface area and can sustain high calcination temperatures. The estrogenic activity (EA) of stock and treated samples was determined by yeast estrogen screen (YES) assay, which is based on human estrogen receptor-transfected yeast strain *Saccharomyces cerevisiae*. The toxicity tests were performed with marine bacteria *Vibrio fischeri* and water fleas *Daphnia magna*. Finally, the photocatalyst stability was examined in a continuous-flow UV irradiated reactor for 25 h on stream.

2. Experimental

2.1. Synthesis of immobilized TiO_2 photocatalyst

TiO_2 was immobilized by impregnating the non-woven glass fiber cloth (Sartorius™, grade MGA) with 0.3 M $TiOSO_4{\cdot}xH_2SO_4{\cdot}xH_2O$ (Sigma–Aldrich) solution. For this purpose, rectangular GF papers of dimensions 6×17 cm were cut and used as received in dip-coating preparation method. The substrate was immersed in the solution of the coating material and simultaneously withdrawn at a constant speed of 3 cm min^{-1} as depicted in the schematic drawing (Fig. S1). After wetting the filter paper, an excess liquid was drained from the surface. The as-prepared GF papers were dried at 60 °C, scrolled and placed in a calcination oven for 1 h at 500 °C. The dip-coating procedure was not repeated and fabricated immobilized photocatalysts were directly applied in photocatalytic oxidation process.

2.2. Characterization of immobilized TiO_2 photocatalyst

The textural, surface and morphological properties of fresh and used photocatalysts were investigated using SEM-EDX, XRD, UV–vis-DR, FTIR and N_2-physisorption. SEM-EDX analyses were performed by field-emission scanning electron microscope (FE-SEM SUPRA 35VP, Carl Zeiss), equipped with energy-dispersive detector (Inca 400, Oxford Instruments). The phase composition of immobilized TiO_2 was determined from the collected X-ray powder diffraction patterns. PANalytical X'pert PRO MPD diffractometer using Cu Kα1 radiation (1.54056 Å) in reflection geometry was applied for the measurement of Bragg diffractions. The data were collected in the range between 10 and 90° in steps of 0.034°. Crystalline phases were identified by comparison with PDF standards from the International Center for Diffraction Data (ICDD).

Diffuse reflectance UV–vis spectra of the bare support, and fresh and used supported TiO_2 were recorded at room temperature using a PerkinElmer Lambda 35 UV–vis spectrophotometer equipped with the RSA-PE-19 M Praying Mantis accessory, which is designed for diffuse reflectance measurements of horizontally positioned powder samples, pastes or rough surface samples. The white reflectance standard Spectralon® was used to perform the instrument background correction in the range of 200–900 nm. The ATR-FTIR spectra were recorded by FTIR analyzer model Frontier 100 (PerkinElmer), equipped with GladiATR VisionTM (PIKE Technologies) accessory that contained a diamond crystal. The obtained spectra were a result of 16 scans with a resolution of 2 cm^{-1} in the spectral range 4000–400 cm^{-1}.

Specific surface area measurements of the photocatalysts were determined from the adsorption isotherms of N_2 at −196 °C within the 0.06–0.30 P/P_0 range using a Micromeritics TriStar II 3020 instrument. This characterization was performed after degassing the samples under N_2 stream (purity 6.0) and programmed bi-level heating, starting with the first heating stage at 90 °C for 60 min and followed by the second heating stage at 180 °C for 240 min. The heating rate was set to 10 °C min^{-1} for both heating stages.

To measure the pH of the point of zero charge (pH_{PZC}), above which the surface is negatively charged, carefully weighed amounts

Table 1
Water-flow regimes used for continuous-flow photocatalytic degradation of BPs, where $Ø_v$, τ and t represent volumetric flow rate, liquid residence time and time on stream, respectively.

	$Ø_v$ (mL min^{-1})	τ (min)	$t_{on\ stream}$ (min)
Regime 1	10.00	25	90
Regime 2	5.00	50	150
Regime 3	2.50	100	300
Regime 4	1.66	150	900

of GF-supported TiO_2 were added sequentially to 50 mL of aqueous 0.005 M NaCl until the pH of the solution did not change with further solid additions. The equilibrium pH at the plateau of the curve corresponds to the pH_{PZC}. The well-mixed cell in which the measurements were performed was thermostated to 25 °C. The pH of fresh and treated solutions was determined by means of pH meter (Methrom, model 827 pH lab).

2.3. Photolytic/photocatalytic experiments

Solutions of bisphenols ($C_0 = 4.38 \times 10^{-5}$ mol L^{-1}) were prepared daily with fresh ultrapure water (18.2 MΩ-cm). Photolytic oxidation experiments of BP solutions were exclusively carried out in a 250 mL batch reactor under irradiation of UV high-pressure mercury lamp (150 W, with a maximum at λ = 365 nm), which was positioned in a water-cooling jacket immersed vertically in the aqueous solution. The BP solutions were thermostated at 20 °C (Julabo, model FP/ME 25), magnetically stirred and continuously aerated with purified air (45 L h^{-1}). Prior to illumination of the reactor content, a 30 min "dark" period was maintained, in order to establish equilibrium of the sorption process. The reactor content was illuminated for 2 and 4 h, and representative 1.5 mL samples were continuously withdrawn. Photocatalytic runs were conducted under the same experimental conditions as photolytic experiments, except that the scroll of glass fiber-supported TiO_2 was immersed into the solution, in a way that the light bulb was surrounded by the photocatalyst. These photo-oxidation tests were conducted in the presence of UV light for 2–8 h. On the other hand, the photocatalytic degradation runs of BPs in a CSTR were subjected to four different water-flow regimes (Table 1), starting with the regime 1 (shortest liquid residence time, τ) and finishing the experiment after 24 h on stream under regime 4 (longest τ). CSTR oxidation runs were performed in equally sized reactor as batch experiments and under the same experimental conditions as stated previously, except that the reactor was equipped with the inflow and outflow of aqueous streams.

2.4. Chemical analyses of aqueous samples

The stock solutions as well as the continuously collected particle-free samples were analyzed for the content of BPA, BPF and BPAF by means of HPLC apparatus (Spectra system™) and PerkinElmer (model Lambda 45) UV–vis spectrophotometer. The HPLC analyses were performed in an isocratic analytical mode, using a 100 mm × 4.6 mm BDS Hypersil C18 2.4 μm column thermostated at 30 °C and equipped with a universal column protection system. The mobile phase was a mixture of methanol and ultrapure water (70:30 volume ratio), and was introduced into the system with a flow rate of 0.5 mL min^{-1}, while an UV detection was fixed at λ = 210 nm. The aforementioned UV–vis spectrophotometer was combined with an 8-cell manual changer for determination of bisphenol concentrations in the aqueous-phase samples. Samples were scanned in the range from 400 to 200 nm with a scan rate of 120 nm min^{-1}. Ion chromatography (IC) on DX-120 Dionex apparatus was performed, in order to determine the content of liberated F^- ions in treated BPAF samples. TOC analyzer (Teledyne Tekmar, model Torch) equipped with a high-pressure NDIR detector was applied to determine the level of mineralization, i.e., the total amount of removed organic substances in withdrawn aqueous-phase samples. A high-temperature catalytic oxidation (HTCO) method was employed (at 750 °C), which subtracted the measured inorganic carbon content from measured total carbon (TC) content, which in this case corresponds to the TOC content. In all analyses, 2–3 repeated measurements were taken for each liquid-phase sample, and the average value of TOC concentration was reported. Leaching of Ti from the photocatalyst during the photocatalytic reaction was verified by inductively coupled plasma mass spectrometry (ICP-MS) analysis of treated aqueous samples.

2.5. Toxicity tests

The toxicity tests of stock and treated BP solutions were performed with marine bacteria *V. fischeri* and water fleas *D. magna*. The freeze-dried luminescent bacteria *V. fischeri* NRRL-B-11177, obtained from the manufacturer (Dr. Lange GmbH, Düsseldorf, Germany), were exposed to polluted samples in two replicates for 30 min at 15 ± 0.2 °C. The luminescence of *V. fischeri* was measured at the start of the experiment (before adding samples) and after 30 min of exposure on a LUMIStox 300 luminometer. The percentage of luminescence inhibition was calculated for each treated sample relative to the luminescence of the control samples. *D. magna* Straus 1820 (Clone A) were obtained from the ECT Oekotoxikologie, Flörsheim, Germany. Twenty water fleas were placed into 3 L aquariums covered with glass plates containing 2.5 L of modified M4 medium at 21 ± 1 °C and illuminated with fluorescent bulbs (approx. 1800 lux) in a 16/8 h light/dark regime. Water fleas were fed twice a week with TetraMin® (20 mg blended in deionised water per aquarium), once a week with instant yeast (5 μg per aquarium) and four times a week with algae *Desmodesmus subspicatus* Chodat 1926 corresponding to 0.13 mg C/daphnia [36]. In the acute toxicity test with water fleas, neonates less than 24 h old were exposed to the stock solutions of BPs and undiluted treated samples in two replicates. After 24 and 48 h of exposure, the immobile daphnids were counted and the percentage was calculated [37].

2.6. Estrogenicity tests

Estrogenic activity (EA) of stock BP solutions and treated samples was determined by YES assay [38]. The human estrogen receptor-modified yeast strain *S. cerevisiae* BJ1991 was used under agreement with John P. Sumpter (Brunel University, UK). Firstly, the aqueous samples containing different amounts of bisphenols and their reaction derivatives were concentrated using the Oasis® HLB 6 cc (500 mg) solid phase extraction (SPE) cartridges (Milford, Massachusetts, USA) and methanol as an eluting solvent [39]. In order to find a relationship between estrogenic activity and successive dilutions of SPE concentrates, serial dilutions were prepared in ethanol and 10 μL aliquots of these solutions were transferred in duplicates to 96-well optically flat-bottom microtiter plates (TPP, MIDSCI, St. Louis, USA) under sterile conditions. After evaporating the ethanol to dryness, 200 μL of the assay medium containing yeast and chromogenic substrate CPRG were dispensed to each hole on the microtiter plate. Each experiment was repeated twice. Validity of the YES assay was confirmed with a positive control (2.6–1.36 μg L^{-1} of 17β-estradiol), a negative control (0.025–1.57 μg L^{-1} of progesterone) and a blank control (yeast exposed to the growth medium and CPRG). The plates were shaken vigorously and incubated in a ventilated heat-chamber (WTW, TS 606/2i) at 34 °C for 46–48 h. The absorbance at 575 and 620 nm was measured on the microtiter plate reader PowerWave XS (BioTek, USA). Relative estrogenic activity (REA) of diluted SPE concentrates was expressed in percent relative to the BPA, BPF and BPAF max-

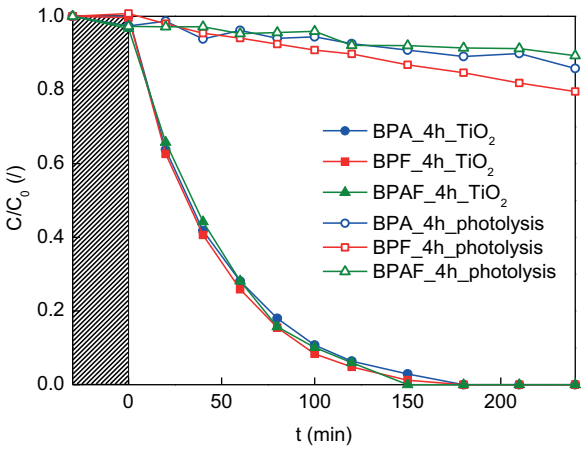

Fig. 2. Photolytic/photocatalytic degradation profiles of BPA, BPF and BPAF aqueous solutions obtained in a batch reactor.

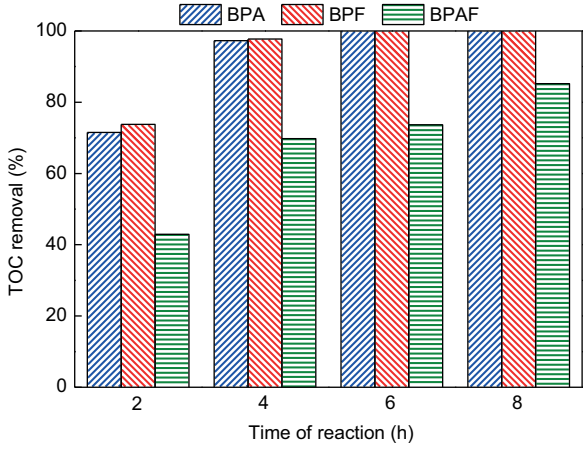

Fig. 3. Total organic carbon (TOC) removals of BPA, BPF and BPAF as a function of reaction time in a batch reactor.

imal responses following the correction of measured absorbances for turbidity.

3. Results and discussion

3.1. Photolytic/photocatalytic experiments in batch reactor

Photolytic experiments, i.e., performed in the absence of a photocatalyst, in a batch reactor demonstrated that BPF possessed the least photo-resistant character among examined BF analogs (Fig. 2). After 4 h of exposure to UV light, roughly 20% of BPF was degraded; in the meantime only 14 and 11% of BPA and BPAF was degraded, respectively. BPF differs from BPA only in virtue of its lack of two methyl groups on the central carbon atom. On the contrary, the two CF_3 groups attached to the central C atom of BPAF permitted the highest photolytic stability among examined BPs. However, the photocatalytic oxidation runs showed very similar behavior; after 3.5 h more than 99% of initial pollutant concentration was degraded. The oxidative decomposition rate of BPs obeyed the pseudo-first-order kinetics, of which the order was BPF ($k' = 2.18 \times 10^{-2}\ min^{-1}$) > BPA ($k' = 2.11 \times 10^{-2}\ min^{-1}$) > BPAF ($k' = 2.09 \times 10^{-2}\ min^{-1}$). The apparent first order rate constants (k') were determined by applying the Langmuir–Hinshelwood (L–H) kinetic model, with the assumption that the reaction takes place on the surface of photocatalyst particles:

$$\ln\left(\frac{C_0}{C}\right) = k' \times t \quad (1)$$

where C_0 represents the initial concentration of the pollutant, C the concentration of the reactant and t the irradiation time. Eq. (1) is a simplified L–H kinetic model that can be applied for mM concentrations $C \ll 1$. k' was given by the slope of the graph ln (C_0/C) versus t. The whole kinetic procedure of photocatalytic degradation of organic compounds in mM concentrations is described in detail in our previous work [40]. Wang et al. [41] reported k' values for BPA removal in horizontal circulating bed photocatalytic reactor (HCBPR) over polyurethane foam (PF)-supported TiO_2. At initial BPA concentration $C_0 = 10$ ppm, temperature (T) = 24.3 °C and 1% (v/v) carrier dosage, k' was about 7-times lower compared to the results obtained in this study.

The difference in adsorption within the first 30 min (before irradiation) between the photocatalyst-free starting solutions (photolytic runs) and the solutions with immersed scroll of photocatalyst (photocatalytic runs) was 0.6% for BPA and BPAF, and 0.9% for BPF, respectively. These amounts of adsorbed bisphenols are indeed negligible for a relatively large geometric area of glass fiber scrolls. Similar photocatalytic degradation profiles could be attributed to comparable adsorption of parent molecules on the catalyst surface (occurring via π–π electron donor–acceptor interactions of benzene rings), thus initiating the same active center of examined BPs. Both fresh and treated solutions of BPA, BPAF and BPF exhibited acidic pH. The pH of fresh BP solutions was in the range from 5.6 to 5.8. The final pH values (after the photocatalytic treatment) were a bit lower and ranged between 4.1 and 4.3. The pH_{PZC} of the GF-supported TiO_2 was determined to be 4.6 (Fig. S2), due to prevailing amount of the borosilicate support, which exhibited pH_{PZC} between 2 and 3 [42]. The active phase (i.e., TiO_2 in the form of anatase) gives pH_{PZC} above 6 [37]. Accordingly, it can be assumed that the immobilized TiO_2 locally exhibited a positively charged surface, due to an excess of protons from acidic aqueous solution. As a result, the negatively charged atoms in molecular structures of BPA, BPF and BPAF were attracted to the TiO_2 surface through coulombic forces. The most negative point charge atoms are oxygen atoms in hydroxyl groups and are easily adsorbed on the TiO_2 surface through electrostatic interactions [43]. The photogenerated •OH radicals, produced from oxidation of water molecules on the TiO_2 surface, are then expected to be the major oxidative agents responsible for degradation of adsorbed organic molecules [44].

The UV–vis spectra (Fig. S3) of photocatalytically treated solutions of BPA, BPF and BPAF confirmed the exceptional oxidation power of TiO_2-based immobilized photocatalyst compared to the photolytic oxidation runs. The spectra of the latter (exposed to UV light either for 2 or 4 h) only slightly deviated from the spectra of fresh solutions of BPs. On the contrary, the characteristic absorption peaks at around 226 and 275 nm diminished rapidly in the presence of the photocatalyst, and approached to the spectrum of pure water. This observation indicates that the water dissolved BPs were not only converted to their low-molecular-weight intermediates, but also effectively transformed into CO_2 and H_2O, as final products of oxidative reaction. More detailed mineralization efficiency is depicted in Fig. 3, in terms of TOC removal as a function of time of illumination with UV light. According to TOC data, it is evidently that BPAF is much less prone to be mineralized compared to other two analogs. Namely, the TOC removal of BPA and BPF was almost complete already after 4 h of photocatalytic oxidation, whereas the TOC conversion of BPAF was not more than 70%. Even the prolongation of time exposed to UV light in the presence of photocatalyst did not bring a significant improvement in mineralization of BPAF; after 8 h of photocatalytic degradation still 14.7% of BPAF derivatives (in terms of TOC) was present in the solution.

Table 2
Remaining TOC and unliberated fluoride contents during BPAF degradation in a batch reactor.

t (h)	2	4	6	8
$TOC_{remaining}$ (%)	57.0	30.1	26.4	14.7
F^-_{bound} (%)	73.9	73.3	70.7	68.5
$F^-_{liberated}$ (mg L^{-1})	1.30	1.33	1.46	1.57

Combining ion chromatography (IC) for determination of released fluoride ion (F^-) and TOC analysis, it was possible to evaluate the percentage of uncleavaged C—F bonds (Table 2). The results showed that after 8 h of photocatalytic treatment, 68.5% of F^- was still bound to carbon atoms. A simple mass balance calculation elucidated that 4 F^- ions per molecule (i.e., 66.6%) remained bound to two C atoms (i.e., 13.3% of carbon in BPAF). These theoretical data are in good agreement with the measured values, revealing that 2/3 of C—F bonds were still intact. In general, carbon-fluorine bonds (C—F, ~116 kcal/mol) are stronger than carbon–hydrogen bonds (C—H, ~99 kcal/mol), providing an increased oxidative and thermal stability of carbon–fluorine compounds compared with the carbon–hydrogen isosteres. Because of the electronegativity difference between carbon and fluorine (2.5 versus 4.0), C—F bonds are more polar, which in turn contributes to the difference in C—F versus C—H bond strengths [45]. Thus, restricted cleavage of strong C—F bonds clarifies, why BPAF and its derivatives are less prone to photocatalytic degradation.

The photodegradation pathways of BPA have been investigated by other researchers [43,46]. It was determined that the two carbon atoms of the benzene rings (para position to OH moiety) bear the highest frontier electron density points and, therefore, are attracted by •OH radicals, causing the cleavage of benzene-rings in BPA [43]. In the initial photo-oxidation, phenol radical ($•C_6H_4OH$) and isopropylphenol radical ($•C(CH_3)_2C_6H_4OH$) are formed and then converted (upon incorporating another •OH radical) to *p*-hydroquinone (HOC_6H_4OH) and 4-hydroxyphenyl intermediates (such as *p*-hydroxybenzaldehyde, *p*-hydroxyacetophenone and 4-hydroxyphenyl-2-propanol), respectively. Moreover, these single-aromatic intermediates are subsequently oxidized through ring-opening reactions into aliphatic acids, such as formic and acetic acids [47]. The absence of methyl groups in BPF influences on the point charges and, therefore, different intermediate products are formed, yielding also different ratio between formic and acetic acids. However, these short chain intermediates were completely transformed to carbon dioxide and water in both BPA and BPF mineralization pathways. On the contrary, the photodegradation mechanism of BPAF is still unclear in its details. Different point charges due to the presence of CF_3 moieties might govern another pathway of photo-oxidation by •OH radicals towards CO_2, H_2O and F^-. Our results pointed out that one F^- ion per CF_3 group can be liberated in the initial stage of photocatalytic treatment, leaving the other two fluorides bound to carbon atom throughout the 8 h photocatalytic run. Obviously, further photocatalytic treatment with this reaction setup would not bring further improvement in TOC reduction and F^- liberation. In view of this imperfection, further photocatalyst improvement and/or addition of sequential advanced water purification techniques would be desired.

3.2. Toxicity tests of fresh and treated solutions of BPA, BPF and BPAF in batch reactor

Progressive photocatalytic degradation of emerging water pollutants may generate reaction intermediates of higher toxicity to aquatic organisms than the parent molecules. As regards to BPAF, this may be the potential concern, since its degradation route was not complete and not much is known about the molecular structure

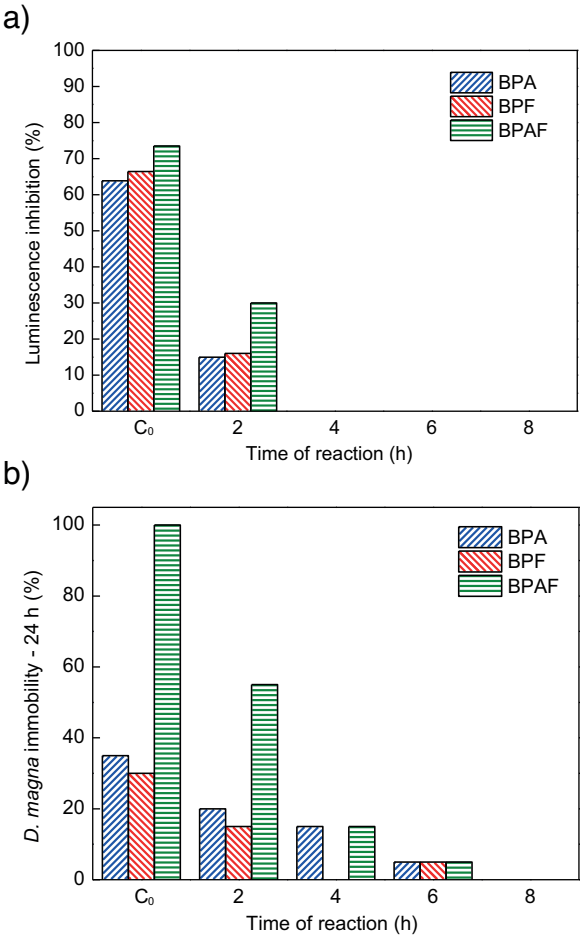

Fig. 4. Toxicities of stock and photocatalytically treated solutions of BPA, BPF and BPAF in the batch reactor to (a) bacteria *Vibrio fischeri* and (b) water fleas *Daphnia magna*.

and toxicity potential of its reaction intermediates. Comprehensive toxicity results of stock and treated BPA, BPF and BPAF solutions are presented in Fig. 4. It is clearly evident that all photocatalytically treated solutions exhibit lower toxicity to both aquatic organisms compared to the starting solutions of BPs. Moreover, luminescence inhibition of marine bacteria *V. fischeri* (Fig. 4a) was diminished more than three times after 2 h of photocatalytic oxidation and completely eliminated in the sample withdrawn after 4 h of treatment. This is in accordance with nearly complete mineralization of BPA and BPF, but also demonstrates that BPAF reaction intermediates (as BPAF degradation was not complete) and liberated fluoride in concentration up to 1.57 mg L^{-1} (Table 2) are non-toxic to these aquatic organisms. The toxicity of the stock and treated solutions to bacteria was slightly more expressed in the presence of BPAF; however, the differences between the three tested BP analogs were insignificant and could be regarded as comparable. On the contrary, compared to BPA and BPF, the acute toxicity of BPAF to *D. magna* (Figs. 4b and S4) was remarkably higher, reaching 100% immobility of daphnids already after 24 h of exposure to initial BPAF solution. Percent of immobile daphnids was nearly halved with photocatalytic oxidation of BPAF solution for only 2 h. Prolonged photodegradation times resulted in yet lower and comparable toxicities (less than 20% of *D. magna* immobility) in both 24 and 48 h acute toxicity tests, respectively. These remaining toxicities can be indeed regarded as negligible and elucidate that liberated fluoride (in quantified concentrations) is benign to daphnids as well. In fact, concentrations of F^- are way too low to elicit toxicity to

these fresh water invertebrates, if we consider the 24 and 48 h EC_{50} values (for immobilization), which vary between 205 and 352 and 98–304 mg L^{-1} F^-, respectively [48].

In addition, these bioassays pointed out a striking difference in sensitivity of aquatic organisms used in this study to evaluate the efficiency in toxicity removal of the photocatalyst. Namely, daphnids were found considerably more sensitive to BPAF than bacteria *V. fischeri*. We assume that fluorinated organic molecules act as enzymatic poisons, inhibiting enzymatic activity (e.g., phosphatases, hexokinase, enolase, succinic dehydrogenase, pyruvic oxidase) and, ultimately, interrupting metabolic processes such as glycolysis and synthesis of proteins [48]. Related findings were reported by Palma et al. [49], accounting bacteria *V. fischeri* for more tolerant organism to organophosphorous (chlorpyrifos), organochlorine (endosulfan sulphate) insecticides and organochlorine (atrazine) herbicides than other aquatic species.

3.3. Estrogenic activity of fresh and treated solutions of BPA, BPF and BPAF in batch reactor

The dose-response curves of stock solutions of BPA, BPF and BPAF were compared with those of photolytically and photocatalytically treated solutions (Fig. 5). Clearly, all the BPs used in this study induced significant levels of β-galactosidase activity in the yeast assay, typically at higher SPE concentrations; thus, they can be considered estrogenic active. When examining the dose–response curves of untreated solutions, it was evident that BPAF was more potent estrogen-like chemical than the other two BP analogs. For example, the relative estrogenic activity of BPAF at concentration factor (CF) 0.3 (i.e., $C = 1.31 \times 10^{-5}$ mol L^{-1}) was already 81%, while the REAs of BPF and BPA were substantially lower, i.e., 33 and 12%, respectively. Such estrogenic activity of these three BP analogs was also determined in the study of Fic et al. [50], reporting a 10-fold higher EC_{50} values for BPAF in comparison to BPA and BPF, respectively, but finding BPAF less potent than 17-β estradiol (E2). From these results it can be deduced that substitutions on propane bridge of BPA regulate estrogenic activity. Concerning BPAF, its CF_3 substituents in place of the 1-methyl group of the propane moiety increased the hormonal activity, while the absence of CH_3 groups in BPF had little effect on estrogenic activity.

Report on binding affinity of HPTE (i.e., an analog of BPAF with CCl_3 group in place of CF_3) to estrogen receptors (ER) revealed similar potency to bisphenol AF in the assays for determination of binding affinity to both ERα and ERβ [51]. BPAF and HPTE differ in chemical structures, but their comparable behavior (similar binding affinity and selectivity) as endocrine disrupting compounds arises from the fact that both have tri-halogenated methyl groups (much more electronegative than the methyl group), which are responsible for substantially different interactions with ERs.

The dose–response patterns of BPAF (Fig. 5c) reminded us that this BP is the most toxic in the comparison, since the β-galactosidase activity at higher concentrations (CF = 5, 10) was hindered, due to the effects on the yeast growth caused by higher acute toxicity of BPAF. Thus, only concentrations with CF up to 2.5 were taken into account. Such behavior was also witnessed with both photolytically treated samples, which further proved a stable character of BPAF in the absence of photocatalyst. On the contrary, the REAs of photocatalytically treated solutions were found restricted. After 2 h of photocatalytic oxidation, the β-galactosidase activity was more than halved, while longer treatment, i.e., for 4 h, completely removed estrogenicity from all the examined samples. Consequently, the dose–response patterns of longer oxidation runs occurred analogous to those of ultra-pure water. In this manner, the YES assay confirmed the photocatalytically treated solutions to be free from estrogenically active reaction intermediates.

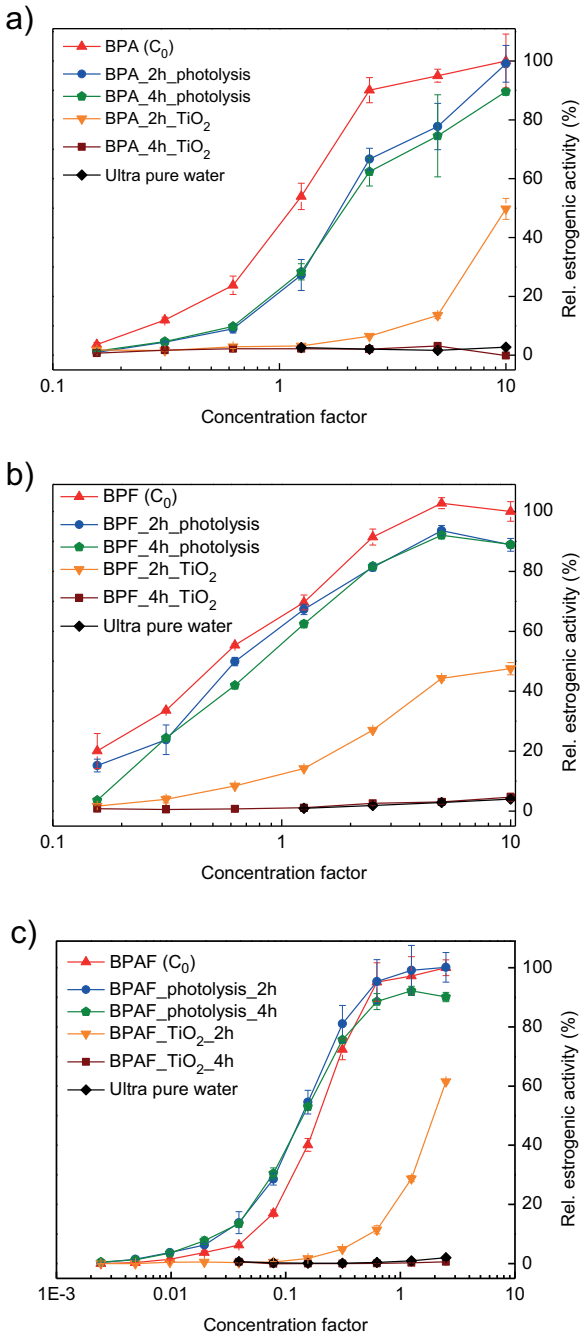

Fig. 5. Relative estrogenic activity of stock and photolytically/photocatalytically treated solutions of (a) BPA, (b) BPF and (c) BPAF in the batch reactor. Lines show trends.

3.4. Photocatalytic experiments in CSTR

Generally, immobilized photocatalysts are intended for long-term removal of aqueous pollutants in continuous-flow photoreactors of various designs. The glass fiber supported TiO_2 photocatalyst was examined in a series of flow regimes (Table 1), starting with the shortest residence time ($Ø_v$ = 10.00 mL min^{-1}) and finishing the run after 24 h time on stream under the longest τ ($Ø_v$ = 1.66 mL min^{-1}). UV–vis spectra of BPA, BPF and BPAF solutions obtained at particular flow regime (or reactor conditions) demonstrated the progress of degradation of these compounds (Fig. S5). In addition, the photocatalytic degradation profiles of BPs as a function of τ are presented in Fig. 6a. The course of photocatalytic oxidation indicated that at

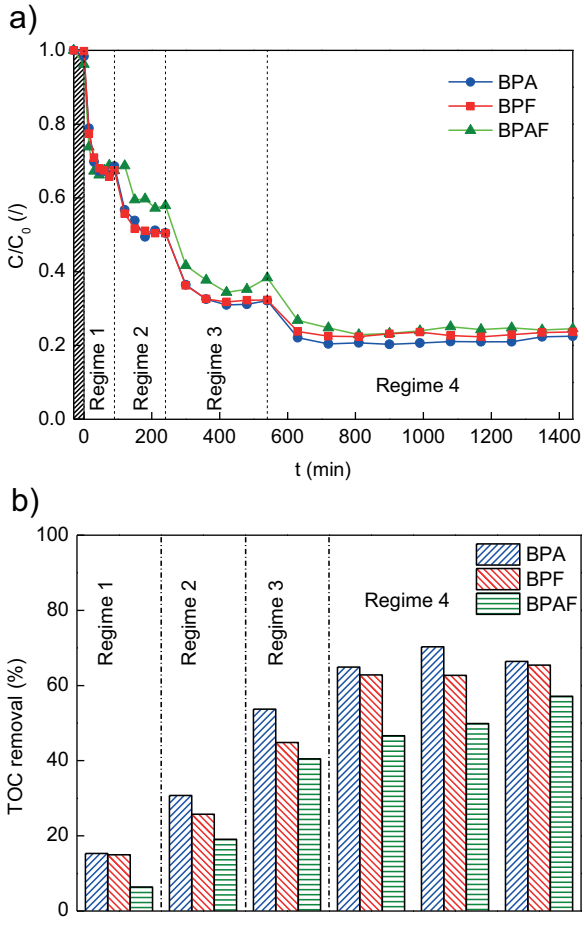

Fig. 6. (a) Photocatalytic degradation profiles of BPA, BPF and BPAF and (b) TOC removal in CSTR as a function of τ.

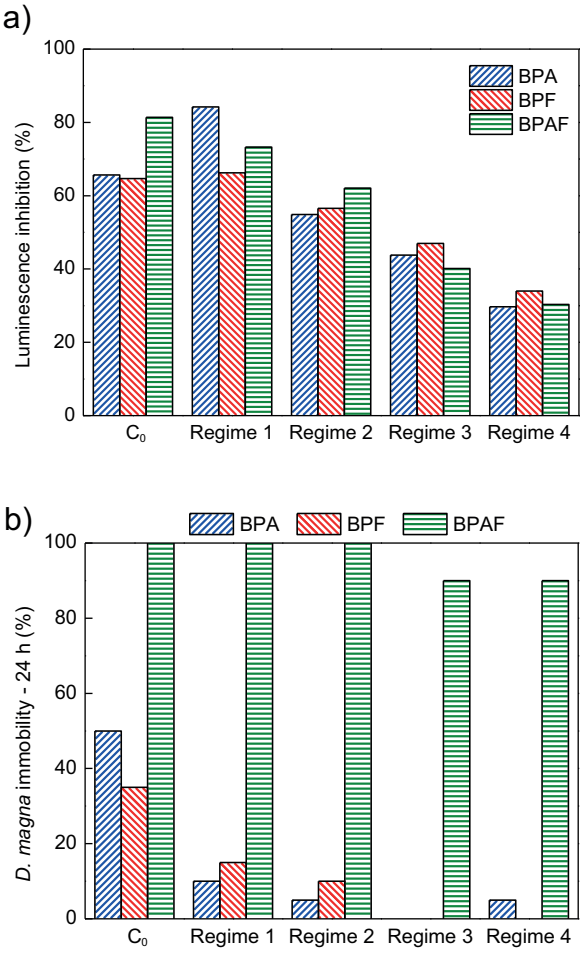

Fig. 7. Toxicities of stock and photocatalytically treated solutions of BPA, BPF and BPAF in CSTR to (a) bacteria *Vibrio fischeri* and (b) water fleas *Daphnia magna*.

least three τ (in terms of time on stream) were needed to achieve steady-state performance (C/C_0 is constant) of the CSTR within the particular flow regime, which is in accordance with the hydrodynamics of this reactor type. Each steady-state run gives, without integration, the reaction rate ($-r_{BP}$) for the conditions within the reactor using the following equation:

$$-r_{BP} = \frac{(C_0 - C)\,\phi_V}{V} \quad (2)$$

where C represents a steady-state concentration and V is reactor volume. The rate constant k of the reaction was determined from the slope of the rate expression in logarithmic form:

$$\log(-r_{BP}) = \log(k) + n\log(C) \quad (3)$$

where n is the reaction order (y-intercept of the rate expression in logarithmic form). Awaited reaction kinetics follow the pseudo-first-order ($n_{BPA} = 0.79$, $n_{BPF} = 0.87$ and $n_{BPAF} = 0.82$), giving similar reaction constants ($k_{BPA} = 2.65 \times 10^{-2}\,min^{-1}$, $k_{BPF} = 2.48 \times 10^{-2}\,min^{-1}$ and $k_{BPAF} = 2.41 \times 10^{-2}\,min^{-1}$) to those obtained in the batch reactor.

The extent of oxidation of bisphenolic compounds in CSTR was dependent on τ. The longer τ, the higher conversion of BPs could be expected. However, conducting the reactions in CSTR towards complete removals was not reasonable, since excessively long τ and, consequently, reactor volume would be required. Operating under regime 4 resulted in approximately 77% conversion of water dissolved BPs. Based on TOC removals determined in each steady-state run (Fig. 6b), substantially lower mineralization of BPAF compared to BPA and BPF, respectively, was attained, which is in accordance with the results obtained in the batch reactor. This signifies that somewhat longer τ of BPAF solution would be needed in CSTR in order to meet mineralization extent of BPA and BPF, respectively. Nevertheless, the immobilized photocatalyst was operating 24 h on stream and showed excellent stability in photocatalytic activity.

3.5. Toxicity tests of stock and treated solutions of BPA, BPF and BPAF in CSTR

With regard to incomplete removal of reactants (i.e., BPA, BPF and BPAF) from aqueous samples in CSTR, the reactor outflow always poses a threat to aquatic environment. The latter was verified by means of acute toxicity tests based on aquatic species from two different trophic levels, i.e. luminescence bacteria *V. fischeri* (Fig. 7a) and water fleas *D. magna* (Figs. 7b and S6). Regardless of the liquid flow rate in CSTR, marine bacteria *V. fischeri* were found equally sensitive to the examined BPs. Luminescence inhibition was gradually diminished along with the conversions and TOC removals of BPs measured at particular liquid flow regime. For instance, operating under regime 4 resulted in 20–25% of unconverted BPs in the reactor outflow, which inhibited *V. fischeri* luminescence for 30% on average. On the other hand, freshwater crustacean *D. magna* was recognized as highly sensitive organism to fluorinated organic molecules even at the highest BPAF conversions obtained under regime 4. In this respect, nearly 90 and 100% of immobile daphnids were found in 24 and 48 h acute toxicity tests, respectively. Hence, these organisms seem to be ideal for bioassays studies of aqueous samples containing BPAF-alike compounds in small quantities. On

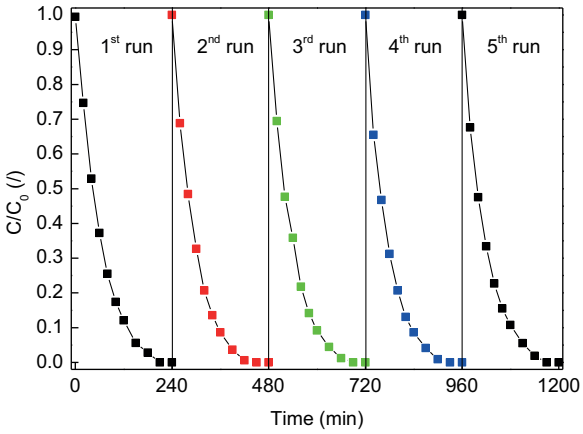

Fig. 8. Recycling of immobilized TiO_2 in the photocatalytic degradation of BPA under UV-light irradiation.

the contrary, BPA and BPF solutions were found significantly less toxic to daphnids and already under regime 1 recognized as negligibly toxic. Further continuous detoxification of these solutions could be reached, if several CSTRs were connected in series. Thus, a series of N (N = whole number) equally sized mixed flow reactors should be closer to the behavior of a plug flow reactor (PFR), which is more efficient than a CSTR for reactions, whose rates increase with reactant concentration, such as nth-order irreversible reactions, $n > 0$ [52].

3.6. Characterization of fresh and used immobilized TiO_2 photocatalyst

The activity and stability of immobilized catalyst are predominantly influenced by physicochemical properties of both catalyst support and deposited active species. Therefore, the as-prepared and used catalysts were thoroughly examined to state whether the long-term photocatalytic oxidation caused any substantial changes in intrinsic properties. First of all, the stability of the immobilized TiO_2 photocatalyst was examined in five successive BPA photo-oxidation experiments in aqueous solution under UV light (Fig. 8). The BPA degradation profiles were almost alike, indicating that the photocatalytic activity of GF-supported TiO_2 was well maintained. Furthermore, the immobilized TiO_2 photocatalyst was subjected to the photocatalytic oxidation run of BPA for 25 h on stream, where two different flow regimes (regime 3 and 4) were altered as depicted in Fig. 9. Both BPA conversion and TOC removal are presented as a function of liquid flow regime. Ideally, the final BPA conversion or TOC removal should meet the conversion/removal extent achieved under the initial flow regime, bearing the same τ. In our case, a slight declination in BPA conversion could be observed, indicating that the photocatalyst suffered from minor deactivation. Several reasons could elicit such outcome. For instance, excessive adsorption of reactants/products on the catalyst surface, and detachment and rearrangement of active species are the usual concerns. The former can be neglected, because the carbon-based elemental analysis of fresh and used photocatalysts did not show any increment of carbon in used photocatalysts, due to the adsorption of carbonaceous organic compounds during the photocatalytic oxidation experiments. In this regard, the photocatalyst investigated in this study possesses efficient intrinsic ability of simultaneous oxidation of carbonaceous deposits.

The BET surface area of bare GFs was exactly 3 $m^2\,g^{-1}$, while the specific surface area of TiO_2-deposited GFs (fresh and used) was around 6 $m^2\,g^{-1}$, due to the increased surface roughness. SEM micrographs of the as-prepared (Fig. 10a) and used (Fig. 10b)

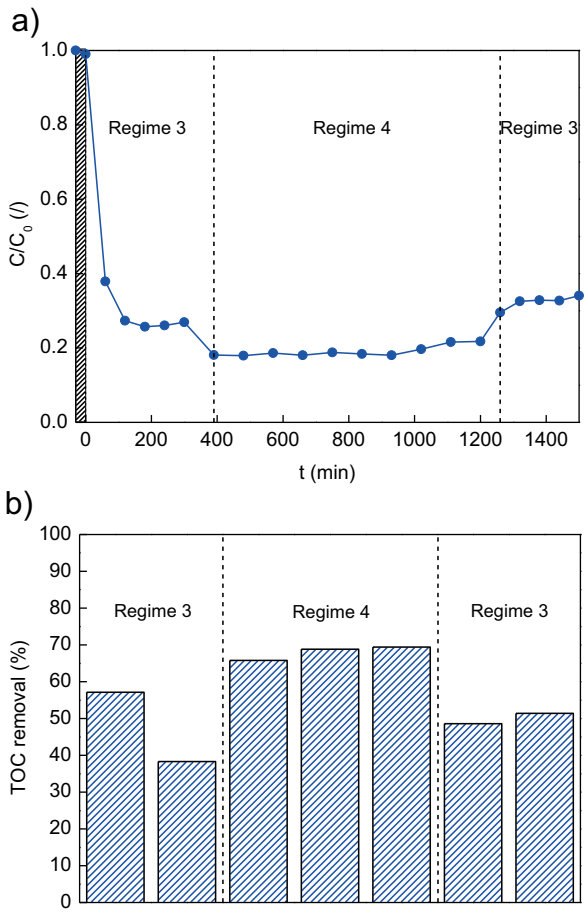

Fig. 9. (a) Photocatalytic degradation of BPA and (b) TOC removal in CSTR as a function of τ during 25 h on stream.

glass fiber-supported TiO_2 photocatalyst indicated that slight declination in catalyst stability could origin from TiO_2 rearrangement/detachment. SEM micrograph of fresh photocatalyst revealed a uniform distribution of TiO_2 particles (~300 nm in diameter) over the surface of glass fibers (0.93 mg of TiO_2 per 1 cm^2 of GFs). However, after 25 h time on stream, TiO_2 particles were approximately 10 times smaller and congested in inter-fiber voids, which implies that some exposed regions of GFs became bare.

The surface functional groups of the support and supported TiO_2 were determined by means of FTIR-ATR analysis (Fig. 11). The major difference between the samples resides in the appearance of characteristic peaks at 1632 cm^{-1}, 3422 cm^{-1} and 3218 cm^{-1}. The former can be assigned to the H—O—H deformation mode and confirms the presence of water molecules. The broad intense band at 3422 cm^{-1} can be attributed to the deformation and stretching vibrations of OH groups of physisorbed water on TiO_2, while the shoulder at 3218 cm^{-1} was ascribed to the strong interaction between Ti ions and OH groups [17].

The X-ray diffraction pattern of fresh immobilized TiO_2 photocatalyst (Fig. 12) revealed the presence of anticipated anatase phase and accompanying impurity, which diffraction peaks were assigned to Na_2SO_4. The latter is water soluble and was simply removed when immersing the photocatalyst into an aqueous solution. Accordingly, the used photocatalysts (i.e., after 4 and 25 h of photocatalytic oxidation runs) exhibited solely anatase Bragg reflections of comparable intensity to that of the as-prepared photocatalyst. Adequately, the diffuse reflectance UV–vis spectra of fresh and used photocatalysts were almost identical and resembled typical TiO_2 response in UV region (Fig. S7). Both of these findings

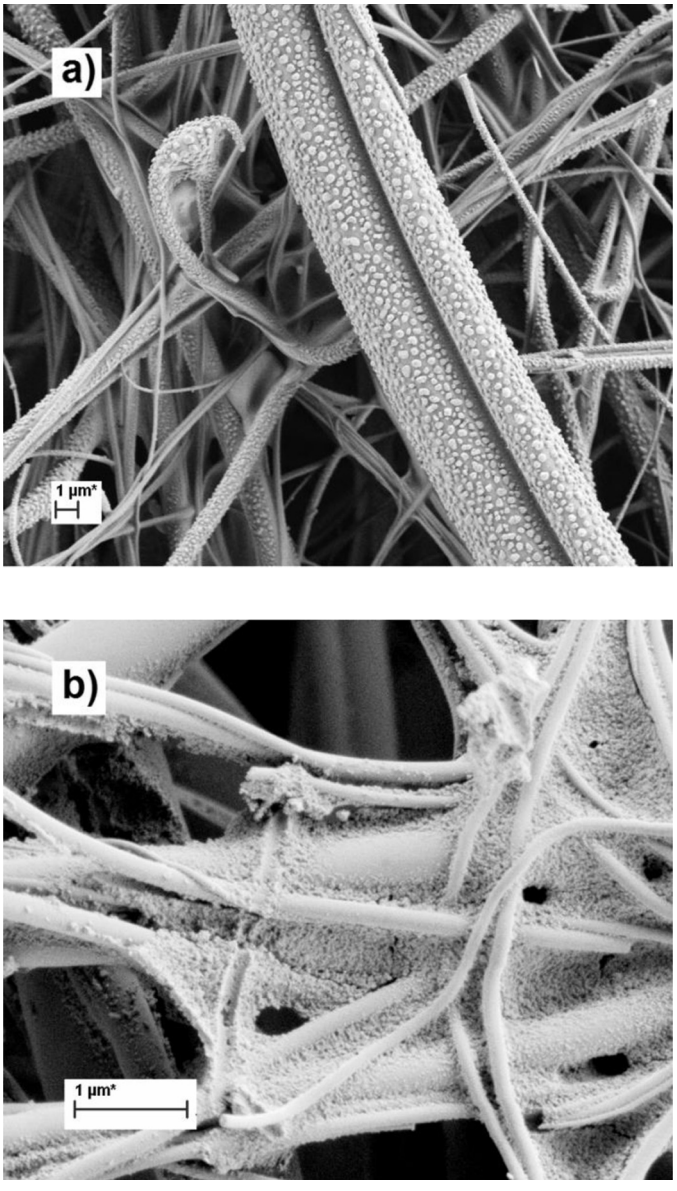

Fig. 10. SEM micrographs of the (a) as-prepared and (b) used glass fiber-supported TiO_2 photocatalyst.

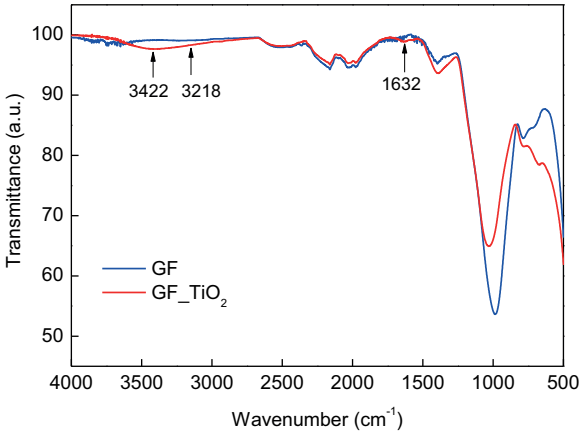

Fig. 11. FTIR spectra of GF and GF-supported TiO_2.

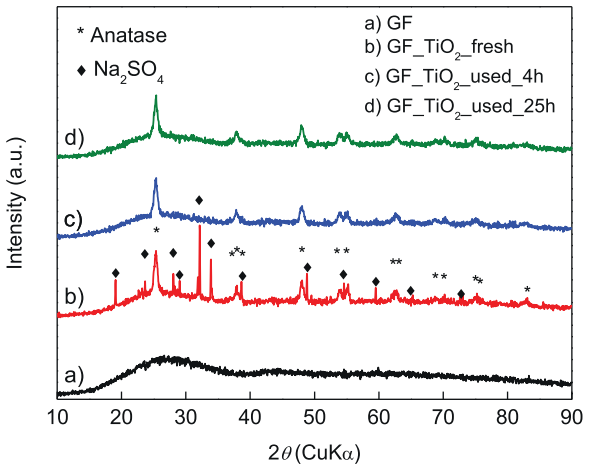

Fig. 12. XRD patterns of the (a) glass fiber support, (b) as-prepared and (c and d) used immobilized TiO_2 photocatalyst after 4 and 25 h on stream, respectively.

imply that the amount of TiO_2 was not really reduced during the photocatalytic oxidation runs. Furthermore, no leaching of titanium (to the detection limit of 0.01 mg/L) was also confirmed by ICP-MS analyses of photocatalytically treated aqueous samples.

The Na_2SO_4 dissolution and liberation of SO_4^{2-} and Na^+ ions only slightly affected the rate of removal of water dissolved BPs, which was also verified in the successive BPA photo-oxidation experiments (Fig. 8). The BPA solution in the second cycle was already free from SO_4^{2-} and Na^+ ions and the reaction rate was slightly increased. Certainly, the relaxation of Na_2SO_4 caused crumbling of larger agglomerates into smaller anatase nanoparticles as seen on SEM images; presumably, this is the reason for slight declination in photocatalyst stability observed in the ultimate stage of continuous photocatalytic oxidation carried out for 25 h (Fig. 9a). Namely, due to the gathering of TiO_2 nanoparticles in heaps, progressively smaller surface area was accessible to reactants (compared to the same particles distributed with interspace over the support), leading to diminished activity of the whole photocatalyst. However, the designed photocatalyst exhibited remarkable activity and carbon selectivity as well as decent stability, which still requires further improvements in future research activities.

4. Conclusions

In this study, glass fiber supported TiO_2 photocatalyst was developed for efficient photocatalytic degradation of endocrine disrupting bisphenolic compounds in both batch and mixed flow reactors. In the batch reactor, solutions containing BPA and BPF were entirely mineralized during photo-assisted oxidation over the advanced photocatalyst. Accordingly, the treated solutions of these two BP analogs were completely detoxified and purified from the estrogenically active compounds. The toxicity and estrogenicity assays of BPAF solution treated photocatalytically for 4 h showed similar results to the other two analogs, although the TOC conversion of this fluorinated BP was not more than 70%. Accordingly, the treated solution contained liberated F^- ions and the remaining fluorinated reaction intermediates, which were found non-toxic and estrogenically inactive. The reason for less successful mineralization of BPAF resides in restricted cleavage of stronger C—F bonds in CF_3 moiety. The toxicity assays based on bacteria *V. fischeri* and invertebrates *D. magna* pointed out a markedly higher sensitivity of the latter aquatic organism to fluorinated bisphenolic molecules, which were believed to act as inhibitors of inherent enzymatic activity. The photocatalytic oxidation runs carried out in CSTR confirmed the basic purpose of the synthesized photo-

catalyst, i.e., a stable photocatalytic activity in a continuous-flow operation. Nevertheless, a minor deficiency in the long-term stability test was noticed, which was most probably provoked with the rearrangement of TiO_2 nanostructures as a consequence of Na_2SO_4 dissolution. The downside of TiO_2 nanoparticle agglomeration was the reduction of effective surface area, leading to reduced formation rate of reactive hydroxyl radicals. Since TiO_2 particles remained attached to the surface of glass fibers, the particle separation process of photocatalytically treated solutions was not necessary like in the case of photocatalytic systems based on suspended photocatalysts.

Acknowledgement

The authors gratefully acknowledge the financial support of the Ministry of Education, Science and Sport of the Republic of Slovenia through Research program No. P2-0150.

Appendix A. Supplementary data

Supplementary data associated with this article can be found, in the online version, at http://dx.doi.org/10.1016/j.apcatb.2015.10.033.

References

[1] J. Schmidt, P. Kotnik, J. Trontelj, Z. Knez, L.P. Masic, Toxicol. In Vitro 27 (2013) 1267–1276.
[2] P. Nicolopoulou-Stamati, L. Hens, V.C. Howard, Endocrine Disrupters: Environmental Health and Policies, Springer, 2001.
[3] C. Chang, Y. Fu, M. Hu, C. Wang, G. Shan, L. Zhu, Appl. Catal. B: Environ. 142–143 (2013) 553–560.
[4] E.M. Rodríguez, G. Fernández, N. Klamerth, M.I. Maldonado, P.M. Álvarez, S. Malato, Appl. Catal. B: Environ. 95 (2010) 228–237.
[5] C. Liao, F. Liu, H.B. Moon, N. Yamashita, S. Yun, K. Kannan, Environ. Sci. Technol. 46 (2012) 11558–11565.
[6] T. Tanaka, K. Yamada, T. Tonosaki, T. Konishi, H. Goto, M. Taniguchi, Water Sci. Technol. 42 (2000) 89–95.
[7] E. Danzl, K. Sei, S. Soda, M. Ike, M. Fujita, Int. J. Environ. Res. Public Health 6 (2009) 1472–1484.
[8] S. Kitamura, T. Suzuki, S. Sanoh, R. Kohta, N. Jinno, K. Sugihara, S. Yoshihara, N. Fujimoto, H. Watanabe, S. Ohta, Toxicol. Sci. 84 (2005) 249–259.
[9] K. Okuda, T. Fukuuchi, M. Takiguchi, S. Yoshihara, Drug Metab. Dispos. 39 (2011) 1696–1703.
[10] M. Audebert, L. Dolo, E. Perdu, J.P. Cravedi, D. Zalko, Arch. Toxicol. 85 (2011) 1463–1473.
[11] D.S. Bermudez, L.E. Gray, V.S. Wilson, Toxicol. Sci. 116 (2010) 477–487.
[12] M. Song, D. Liang, Y. Liang, M. Chen, F. Wang, H. Wang, G. Jiang, Chemosphere 112 (2014) 275–281.
[13] Y. Sui, N. Ai, S.H. Park, J. Rios-Pilier, J.T. Perkins, W.J. Welsh, C. Zhou, Environ. Health Perspect. 120 (2012) 399–405.
[14] Y. Feng, J. Yin, Z. Jiao, J. Shi, M. Li, B. Shao, Toxicol. Lett. 211 (2012) 201–209.
[15] H. Melcer, G. Klečka, Water Environ. Res. 83 (2011) 650–666.
[16] E. Kusvuran, D. Yildirim, Chem. Eng. J. 220 (2013) 6–14.
[17] B. Erjavec, R. Kaplan, P. Djinovic, A. Pintar, Appl. Catal. B: Environ. 132 (2013) 342–352.
[18] R.A. Torres, F. Abdelmalek, E. Combet, C. Pétrier, C. Pulgarin, J. Hazar. Mater. 146 (2007) 546–551.
[19] J. Ng, X. Wang, D.D. Sun, Appl. Catal. B: Environ. 110 (2011) 260–272.
[20] A. Zhang, Y. Li, Sci. Total Environ. 493 (2014) 307–323.
[21] Y. Liu, X. Zhang, F. Wu, Appl. Clay Sci. 49 (2010) 182–186.
[22] L. Zhang, J. Lv, T. Xu, L. Yang, X. Jiang, Q. Li, Sep. Purif. Technol. 116 (2013) 145–153.
[23] Z. Lu, K. Lin, J. Gan, Environ. Pollut. 159 (2011) 2546–2551.
[24] K. Yamada, N. Ikeda, Y. Takano, A. Kashiwada, K. Matsuda, M. Hirata, Environ. Technol. 31 (2010) 243–256.
[25] J.C. Crittenden, J. Liu, D.W. Hand, D.L. Perram, Water Res. 31 (1997) 429–438.
[26] J. Su, H. Yu, X. Quan, S. Chen, H. Wang, Appl. Catal. B: Environ. 138–139 (2013) 427–433.
[27] A. Phuruangrat, A. Maneechote, P. Dumrongrojthanath, N. Ekthammathat, S. Thongtem, T. Thongtem, Mater. Lett. 159 (2015) 289–292.
[28] U.I. Gaya, A.H. Abdullah, J. Photochem. Photobiol. C: Photochem. Rev. 9 (2008) 1–12.
[29] R.A.R. Monteiro, A.M.T. Silva, J.R.M. Ângelo, G.V. Silva, A.M. Mendes, R.A.R. Boaventura, V.J.P. Vilar, J. Photochem. Photobiol. A: Chem. 311 (2015) 41–52.
[30] C.C. Pei, W.W.-F. Leung, Appl. Catal. B: Environ. 174–175 (2015) 515–525.
[31] E.J. Wolfrum, J. Huang, D.M. Blake, P.-C. Maness, Z. Huang, J. Fiest, W.A. Jacoby, Environ. Sci. Technol. 36 (2002) 3412–3419.
[32] E. Sogaard, Chemistry of Advanced Environmental Purification Processes of Water: Fundamentals and Applications, Elsevier Science, 2014.
[33] A.Y. Shan, T.I.M. Ghazi, S.A. Rashid, Appl. Catal. A: Gen. 389 (2010) 1–8.
[34] M.F.J. Dijkstra, A. Michorius, H. Buwalda, H.J. Panneman, J.G.M. Winkelman, A.A.C.M. Beenackers, Catal. Today 66 (2001) 487–494.
[35] L.L.P. Lim, R.J. Lynch, S.I. In, Appl. Catal. A: Gen. 365 (2009) 214–221.
[36] N. Schweitzer, G. Fink, T.A. Ternes, K. Duis, Aquat. Toxicol. 97 (2010) 304–313.
[37] B. Erjavec, T. Tišler, R. Kaplan, A. Pintar, Ind. Eng. Chem. Res. 52 (2013) 12559–12566.
[38] E.J. Routledge, J.P. Sumpter, Environ. Toxicol. Chem. 15 (1996) 241–248.
[39] M. Bistan, R. Logar, T. Tišler, Cent. Eur. J. Biol. 6 (2011) 829–837.
[40] R. Kaplan, B. Erjavec, A. Pintar, Appl. Catal. A: Gen. 489 (2015) 51–60.
[41] R. Wang, D. Ren, S. Xia, Y. Zhang, J. Zhao, J. Hazar. Mater. 169 (2009) 926–932.
[42] D.L. Harame, L.J. Bousse, J.D. Shott, J.D. Meindl, IEEE Trans. Electron Device 34 (1987) 1700–1707.
[43] N. Watanabe, S. Horikoshi, H. Kawabe, Y. Sugie, J. Zhao, H. Hidaka, Chemosphere 52 (2003) 851–859.
[44] W.Y. Teoh, J.A. Scott, R. Amal, J. Phys. Chem. Lett. 3 (2012) 629–639.
[45] S.K. Khetan, T.J. Collins, Chem. Rev. 107 (2007) 2319–2364.
[46] K. Nomiyama, T. Tanizaki, T. Koga, K. Arizono, R. Shinohara, Arch. Environ. Contam. Toxicol. 52 (2007) 8–15.
[47] W.-T. Tsai, M.-K. Lee, T.-Y. Su, Y.-M. Chang, J. Hazar. Mater. 168 (2009) 269–275.
[48] J.A. Camargo, Chemosphere 50 (2003) 251–264.
[49] P. Palma, V.L. Palma, R.M. Fernandes, A.M.V.M. Soares, I.R. Barbosa, B. Environ, Contam. Toxicol. 81 (2008) 485–489.
[50] A. Fic, B. Žegura, D. Gramec, L.P. Mašič, Chemosphere 112 (2014) 362–369.
[51] A. Matsushima, X. Liu, H. Okada, M. Shimohigashi, Y. Shimohigashi, Environ. Health Perspect. 118 (2010) 1267–1272.
[52] O. Levenspiel, Chemical Reaction Engineering, Wiley, 1999.